

Table of Contents

Thesis Summary	3
Abstract	4
1 Introduction	5
2 Data	7
2.1 <i>Data Used</i>	7
2.2 <i>Method for Obtaining Data</i>	9
3 Fitting	10
4 Results	12
5 Conclusions	20
References	21

Thesis Summary

Distant quasars, nuclei of active galaxies, are often redder and dimmer than average quasars. This is partly due to interstellar dust in galaxies in the line of sight between the observer and the quasar. In this work, the observed spectra of quasars selected because of gaseous absorbers in sightline are analyzed and fit using a template spectrum of a quasar combined with extinction to fit the spectrum. From these fits, it can be determined whether the observed spectrum was reddened and dimmed and to what extent. Looking at the interstellar reddening and extinction of quasars helps with understanding the type of dust in the distant galaxies in front of the quasar and how it compares to dust in our galaxy.

Abstract

Interstellar dust in galaxies has a profound effect on the galaxies' light output and apparent properties as well as on the physical processes connected to star formation. Therefore, to understand the true properties of the galaxies around us, it is important to understand the dust in those galaxies and compare it to the dust in our galaxy. To do this, we study the effects of dust on background quasars by analyzing interstellar reddening and extinction. It has been shown that many quasars look redder and dimmer than the average quasar when observing them from Earth, due to the dust in our line of sight. In this project, we analyze observed spectra of quasars with previously identified moderately strong gaseous absorbers along the sightline and compare them to a template quasar spectrum to see if the observed spectrum was dimmed or reddened by the dust in galaxies located along the line of sight. We do this by fitting the observed spectra to the characteristic quasar template spectrum combined with three different extinction curves representative of the Milky Way ($R_V = 3.08$), Large Magellanic Cloud ($R_V = 2.76$), and Small Magellanic Cloud ($R_V = 2.74$). Looking at the best fit E_{B-V} value and the smallest reduced χ^2 value, we determine which extinction curve best fits the observed quasar's continuum in the UV-optical part of the spectrum. It was found that most of the E_{B-V} values were negative and close to 0, which meant that there was not a lot of dust in the foreground of the quasars to cause reddening.

Keywords: quasar, extinction, dust, interstellar medium, reddening, galaxy, spectrum

1 Introduction

The spectra of distant quasars are obscured by dust clouds from galaxies situated in front of the quasar in the line of sight of the observer. A quasar is a nucleus of an active galaxy with a central accreting super massive black hole in which the center is extremely luminous and brighter than the rest of the galaxy. In the advanced stages of a star's formation, dust is released in the interstellar medium, or space between star systems in a galaxy (Jones, 2009). It could be ejected into the medium by stellar explosions (supernovae) or outflows and is subjected to grain processing in the interstellar medium. This dust is different from the organic dust commonly found on Earth. Interstellar dust is composed of small, solid particles, smaller than the common dust with particle sizes measured in units of microns or Angstroms ($1 \text{ \AA} = 10^{-10} \text{ m} = 10^{-4} \text{ \mu m}$). Each particle is about one nanometer to one micrometer in diameter. Interstellar dust could be made of carbon rich compounds, silicates, or other types of chemical compositions such as metallic oxides (Jones, 2009). Dust can even exist in outer part of the galaxies, including the circumgalactic medium (CGM).

Although dust makes up only about 1% of the mass of the interstellar medium, it is important to understand due the effects it has on interstellar gas and its functions in the interstellar medium (Zhuravlev, 2020). Dust shields the gas so it can form and retain molecular hydrogen. It cools the gas to facilitate the hydrogen and serves as a catalyst for molecular formation. It also shields the gas from ionizing radiation so that there would be no disassociation of molecules. Gravitational collapse is a contraction of any object due to its gravity which brings matter towards the center of gravity. Dust can heat and cool interstellar gas and the dust grains provide a site where molecules can form (Juvela et al., 2020). Understanding dust and comparing it to dust in our galaxy is important since dust is instrumental in star formation.

COMPARING DUST IN OTHER GALAXIES TO DUST IN OUR GALAXY

Dust affects background objects by dimming them or by making them look redder. The dimming is called extinction while the reddening is known as interstellar reddening. The magnitude of these effects on quasars and stars and galaxies are due to the dust's composition, dust abundance or column density, and geometry of the dust and stars relative to each other (Cousin et. al, 2019). The dust grain size affects the dimming and reddening of the quasars since the dust absorbs and scatters blue and ultraviolet light more than red light. Thus, different dust clouds with different dust grain sizes will affect the quasars in different ways. In addition to extinction, there are also specific absorption and emission features such as the 2175 Å bump which results from a given chemical composition and grain morphology of the dust.

Three extinction curves, extinction as a function of wavelength, were used to analyze the effects of interstellar reddening and dimming on the observed quasar. These are representative of the dust in the Large Magellanic Cloud (LMC), Small Magellanic Cloud (SMC), and the Milky Way (MW). Each galaxy has a different dust grain type that differs by size and therefore is subject to a different average R_v value, defined as

$$R_v = \frac{A_V}{E_{(B-V)}} \quad (1)$$

Here, the denominator $E_{(B-V)} = A_B - A_V$ where A_B is the extinction in magnitudes in the blue band and A_V is the extinction in magnitudes in the visible band (Mörtsell, 2013). Dust is not homogenous even in a galaxy, so each region in a galaxy could have a different R_v value. MW has an average R_v value of 3.08, LMC2 has an average R_v value of 2.76, and SMCbar has an average R_v value of 2.74. These values are based on the extinction curves determined from observations of a large number of stars in each galaxy. The extinction curve LMC2 is for the

COMPARING DUST IN OTHER GALAXIES TO DUST IN OUR GALAXY

Large Magellanic Cloud supershell region, while the SMCbar extinction curve is for the dust in the optical bar region of the SMC.

These different curves differ in the strength of the 2175 Å bump and in the steepness of the far-UV rise (see Fig. 1).

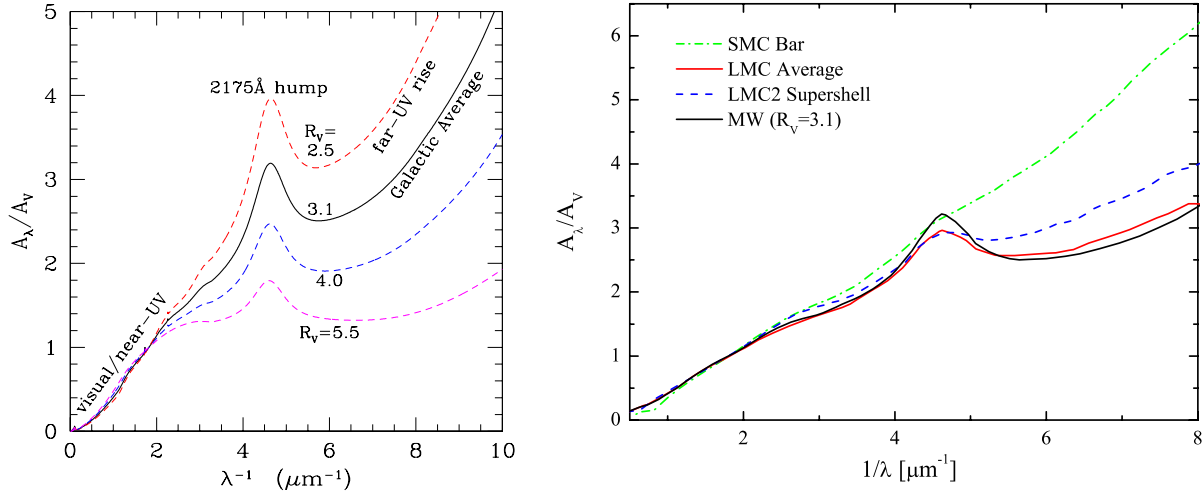


Figure 1 Left: Interstellar extinction curves in the Milky Way for different values of R_V . Higher values of R_V produce a flatter rise in the far-UV (large $1/\lambda$). Right: A comparison of the Milky Way, LMC2 supershell, and SMC bar extinction curves. Also shown is the extinction curve for the LMC. The different curves differ in the strength of the 2175 Å bump and the far-UV rise. Both panels are adopted from Li et al. (2015).

2 Data

2.1 Data Used

Table 1 shows the quasars studied including their emission and foreground galaxy absorption redshifts which are used when analyzing the quasar spectra.

	NED Name	Absorber redshift (Z_{abs})	Emission redshift (Z_{em})	ION	log Ncol
1	PG 0003+158	0.366	0.45	HI	18.40
2	UM 321	0.3989	1.07	HI	18.81
3	LBQS 0256-000	1.1984	3.377	MgII	-
4	3C 232	0.005	0.53	MgII	-
5	MRK 0132	1.6842	1.76	HI	18.89
6	[HB89] 1115+080C	1.7353	1.722	HI	18.03
7	PG 1206+459	0.9254	1.155	HI	18.43

COMPARING DUST IN OTHER GALAXIES TO DUST IN OUR GALAXY

8	LBQS 1229-0207	0.3953	1.038	MgII	-
9	PG 1241+176	0.9927	1.283	HI	18.05
10	SBS 1259+593	0.0464	0.472	HI	18.11
11	[HB89] 1331+170	1.7605	2.097	HI	20.79
12	PG 1338+416	1.0973	1.204	HI	18.48
13	UM 632	0.8903	2.522	MgII	-
14	SDSSJ170100.61+641209.0	2.4394	2.74	HI	18.62
15	SBS 1704+608	0.3646	0.371	HI	19.10
16	OI363	0.0912	0.635	-	-

Table 1 shows the list of objects that were studied in this project which were selected because they had a previously identified, moderately strong, gas-rich absorption system along the sightline. The observed optical spectrum of each quasar listed above was downloaded from the Sloan Digital Sky Survey archive (<http://skyserver.sdss.org/dr16>), and included the wavelength, flux, and uncertainty of the flux. The wavelength was in units of Angstroms and the flux was in cgs units (Flux is the energy received from the quasar per second per area per Å.). The observed spectra for each quasar in Table 1 in optical, infrared (IR), and ultraviolet (UV) wavelengths were compiled by our group using data downloaded from the Sloan Digital Sky Survey, the Spitzer Space Telescope, and the Hubble Space Telescope, respectively. In this project, we focus only on the optical wavelengths from around 4000 to 9000 Å. Quasars in the optical and infrared regions have different template spectra.

A template spectrum, assumed to be the quasar's intrinsic spectrum, is the quasar spectrum before any light is absorbed and scattered by anything in the foreground (see Figure 2). It was made from thousands of quasar spectra that were obtained from the Sloan Digital Sky Survey and averaged by Sloan. In this project, the template spectrum was used as a reference for the observed spectra for comparison and to analyze the effects of dust on the quasar spectrum.

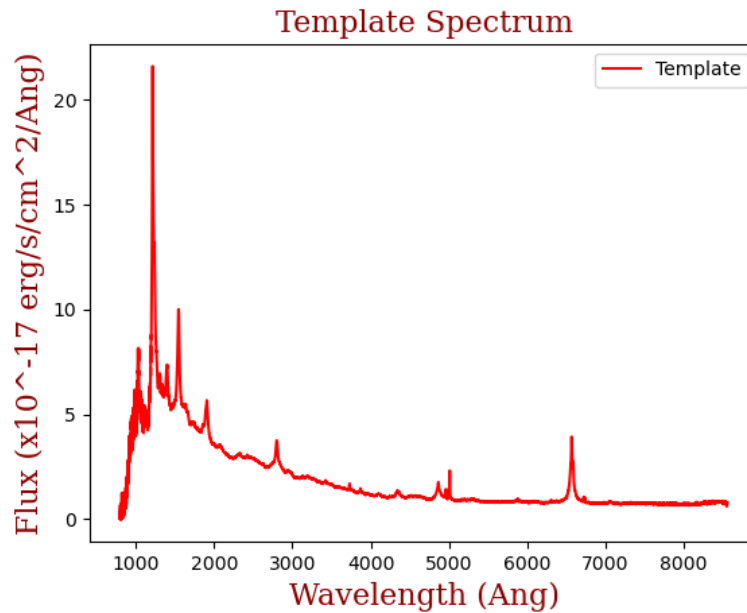


Figure 2 is the template spectrum used when fitting objects in the optical wavelengths. This was obtained from the Sloan Digital Sky Survey.

The goal of this project was to find which extinction curve best fits the continuum of the quasar's observed spectrum, i.e. the region in between the absorption and emission lines. Windows were made to exclude any narrow emission and strong absorption features in the observed spectrum so as to determine the continuum accurately. The emission features come from the quasar itself, while the absorption features come from atomic and molecular gas that is found in front of the quasar. This assumes that the expected central wavelength of the redshift 2175 Å bump of the foreground absorber does not lie directly on top of a strong emission line from the quasar (which is the case for all absorbers in our sample).

2.2 Method for Obtaining Data

As explained before, the template spectrum adopted for the quasars in the optical region was derived from the Sloan digital sky survey. However, the template for quasars in the infrared region are obtained from Hatziminaoglou et al. (2005).

3 Fitting

To decide which extinction curve best fits the spectrum, a code was run on each of the observed quasar spectra curves to see how it varies compared to the template spectrum and by what factor the template should be renormalized to fit the spectrum. To find the most accurate flux renormalization factor, the template was shifted into the observed frame of the quasar using:

$$\frac{\lambda_{obs}}{1 + z_{em}} = \lambda_{rest} \quad (2)$$

where λ_{obs} is the observed wavelength of the observed spectrum, z_{em} is the emission redshift of the quasar, and λ_{rest} is the corresponding wavelength in the rest-frame of the quasar. Then, the flux renormalization factor was calculated based on the ratio:

$$\frac{\text{observed flux at } \lambda_{obs}}{\text{template flux at } \lambda_{rest}} = \text{flux factor} \quad (3)$$

where the flux factor used to multiply by the quasar template to shift it to fit the observed spectrum. This does not give the exact flux factor though, partly because of dust extinction effects, but is a good starting point. The template spectrum is only shifted up and down using the flux factor, but then is reddened using the extinction curve so it can fit the observed spectrum.

The code is run for each object using each of the extinction curves for a grid of values of flux normalization in steps of 0.5 and E(B-V) in steps of 0.01. For each flux factor and E(B-V) value

COMPARING DUST IN OTHER GALAXIES TO DUST IN OUR GALAXY

in the grid, the predicted flux is calculated after including the effect of reddening the quasar template by dust at the absorber redshift and the corresponding χ^2 is calculated as:

$$\chi^2 = \sum \left(\frac{f_{\text{observed}} - f_{\text{predicted}}}{\text{error in } f_{\text{observed}}} \right)^2 \quad (4)$$

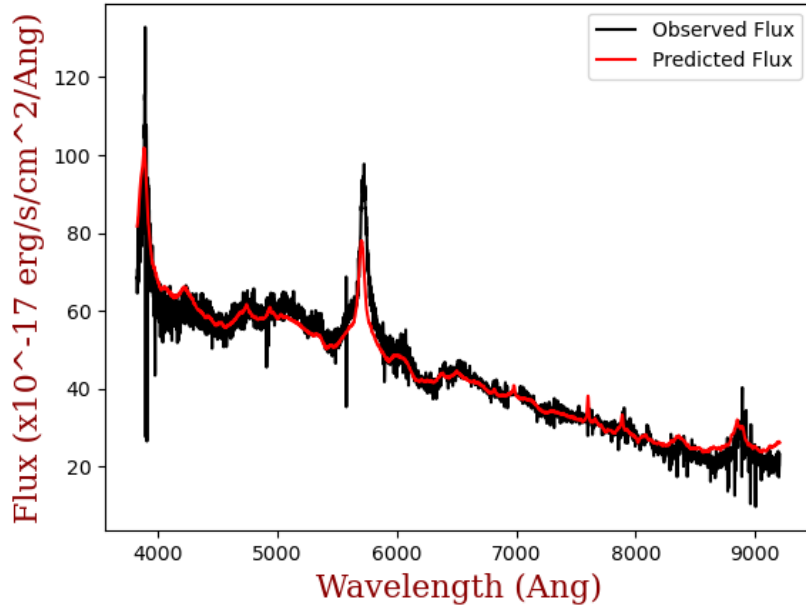
The corresponding reduced χ^2 is given by $\chi_v^2 = \chi^2/(n-1)$, where n is the number of points in the observed spectrum of the quasar. A perfectly constrained fit would yield $\chi_v^2 = 1$.

After running the code on the quasar using each of the extinction curves, the minimum reduced χ^2 value is found for each extinction curve template. Therefore, each object has a minimum reduced χ^2 value for each extinction curve. The smallest of these minimum reduced χ^2 value then determines which extinction curve gives the best fit.

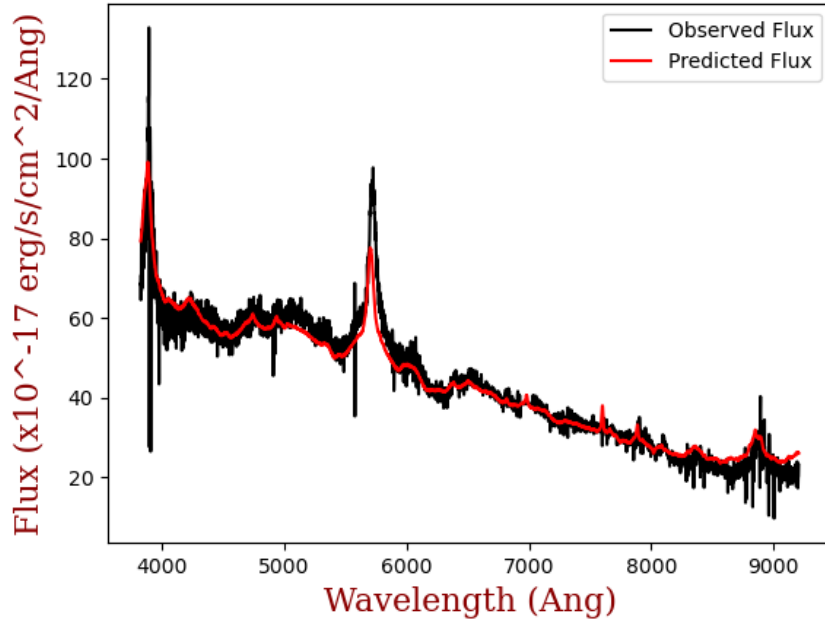
4 Results

Figures 3, 4, 5 show examples of our fitting for 3 different quasars.

LBQS 1229-0207 Flux vs Wavelength: SMCbar



LBQS 1229-0207 Flux vs Wavelength: LMC2



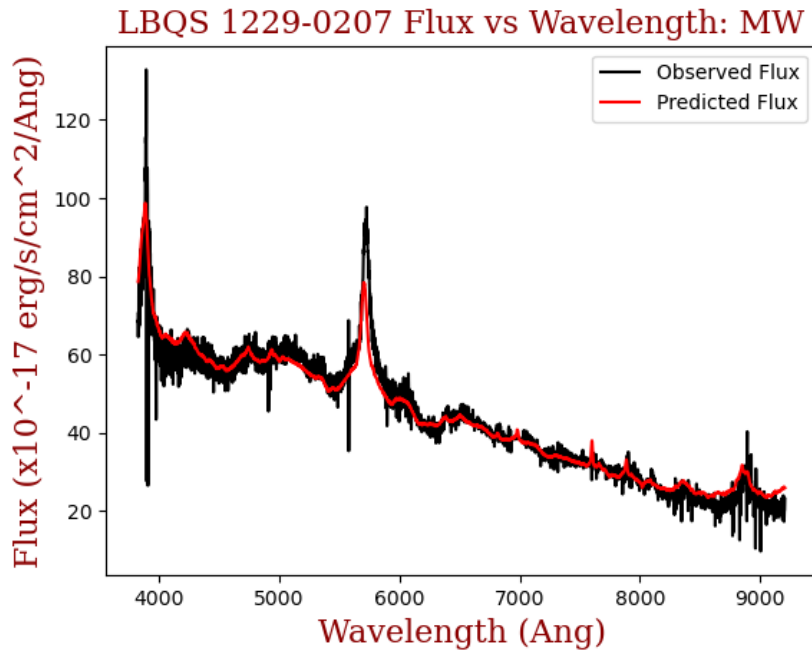
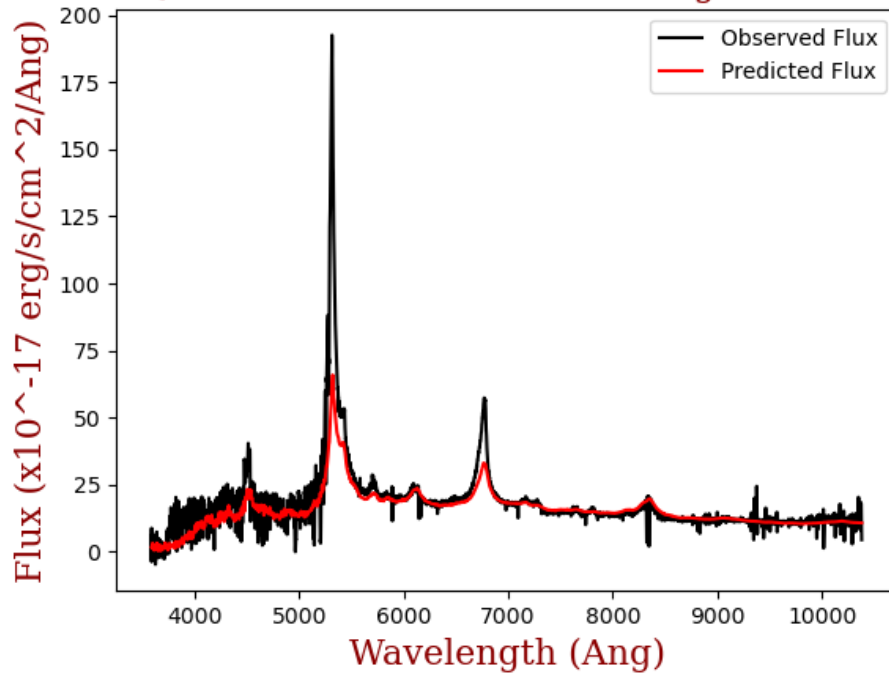


Figure 3 shows the observed spectrum of LBQS 1229-0207 compared to the template file from the Sloan Digital Sky Survey. Also shown are the fits of the spectrum using the three extinction curves: SMCbar (flux norm value = 25.0, $E(B-V) = 0.06$, minimum reduced $\chi^2 = 2.78$); LMC2, (flux norm value = 32.5, $E(B-V) = 0.12$, minimum reduced $\chi^2 = 2.68$); Milky Way (flux norm value = 44.5, $E(B-V) = 0.17$, minimum reduced $\chi^2 = 2.45$). The rest wavelength for this object ranges from about 2744 Å to about 6597 Å.

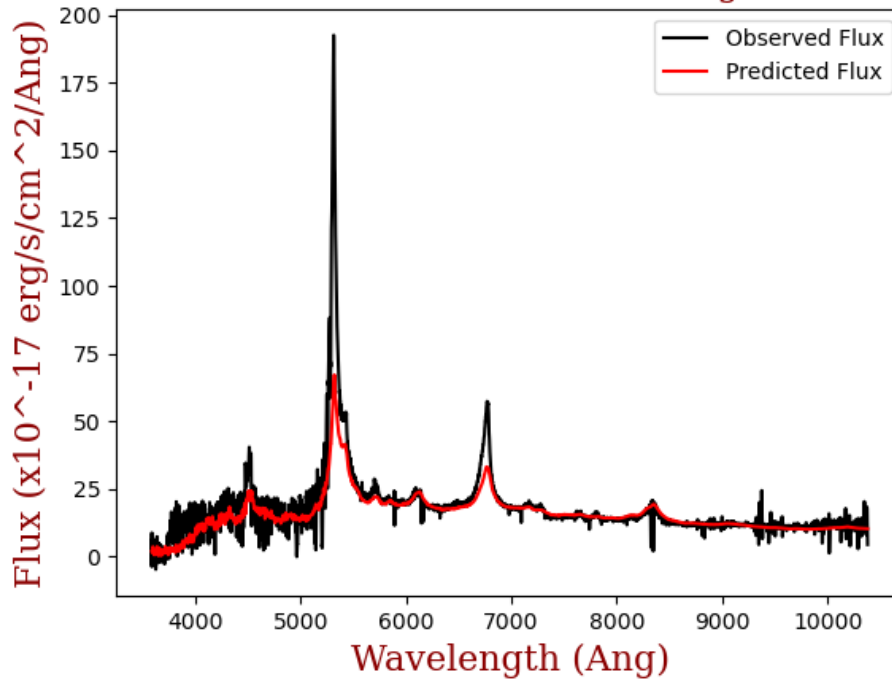
Figure 3 shows an example of our fitting for a quasar that is reddened by dust. From Table 2, it is shown that the best fit E_{B-V} values for this object were positive indicating an extinction is required. From the panels shown in Fig. 3 the observed flux, black curve, is less steep in the blue range (below about 5500 Å) than in the red range in all three of the graphs of the extinction curve fits. This means that the quasar was reddened. The best fit in this case is provided by the Milky Way extinction curve.

COMPARING DUST IN OTHER GALAXIES TO DUST IN OUR GALAXY

LBQS 0256-0000 Flux vs Wavelength: SMCbar



LBQS 0256-0000 Flux vs Wavelength: LMC2



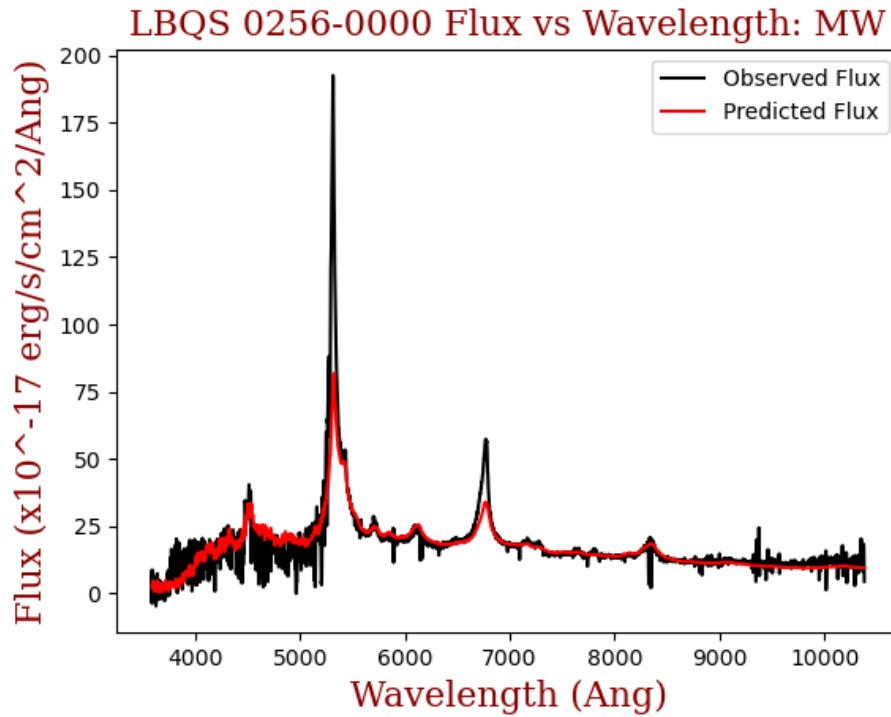
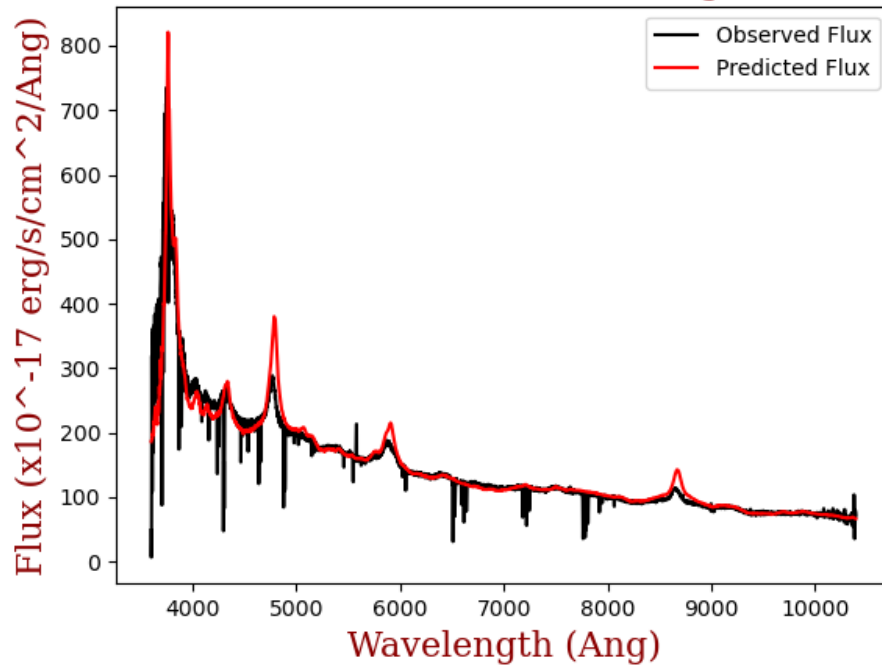


Figure 4 shows the observed spectrum of LBQS 0256-0000 compared to the template file from the Sloan Digital Sky Survey. There also the fits of the spectrum using the three extinction curves: SMCbar (flux norm value = 4.0, $E(B-V) = 0.04$, minimum reduced $\chi^2 = 5.14$); LMC2 (flux norm value = 4.0, $E(B-V) = 0.04$, minimum reduced $\chi^2 = 3.91$); Milky Way (flux norm value = 2.50, $E(B-V) = -0.06$, minimum reduced $\chi^2 = 3.87$). The rest wavelength for this object ranges from about 1633 Å to about 4721.7 Å.

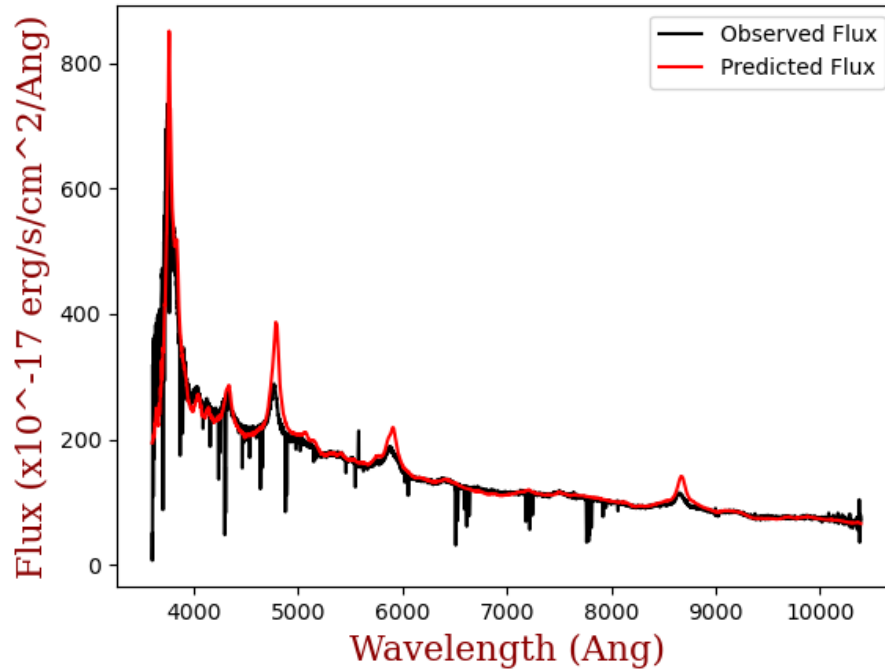
Figure 4 shows our fitting results for the quasar LBQS 0256-0000. It can be seen that the steepness of the observed spectrum is not much different on the blue side than on the red side. This is also shown in Table 2 where the best fit E_{B-V} values are slightly positive for this quasar when fit with the SMCbar and LMC2 extinction curves, but negative when fit with the Milky Way extinction curve. (The negative values do not have a physical significance and suggest a slight mismatch between the template spectrum and the fitted quasar spectrum.) It is also important to note that the Milky Way extinction curve was the best fit for this quasar. Thus, the dust in the foreground absorber did not have much of an effect on the quasar with regards to interstellar dimming and reddening.

COMPARING DUST IN OTHER GALAXIES TO DUST IN OUR GALAXY

[HB89] 1331+170 Flux vs Wavelength: SMCbar



[HB89] 1331+170 Flux vs Wavelength: LMC2



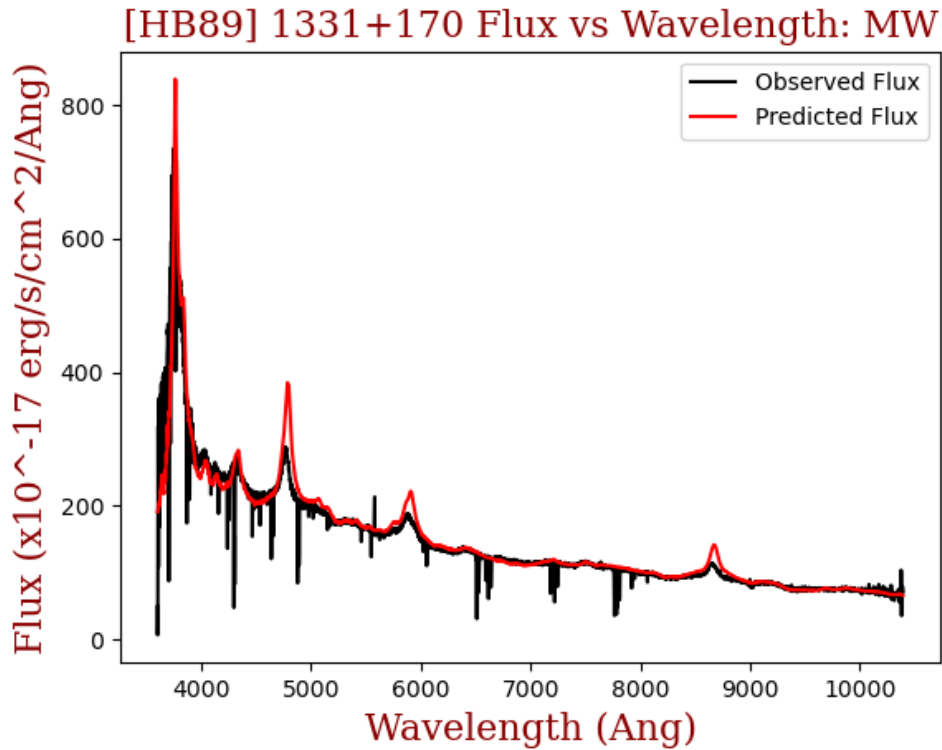


Figure 5 shows the observed spectrum of [HB89] 1331+170 compared to the template file from the Sloan Digital Sky Survey. There also the fits of the spectrum using the three extinction curves: SMCbar (flux norm value = 38.0, $E(B-V) = -2.9E-8$, minimum reduced $\chi^2 = 4.47$); LMC2 (flux norm value = 35.9, $E(B-V) = -0.01$, minimum reduced $\chi^2 = 3.85$); Milky Way (flux norm value = 35.9, $E(B-V) = -0.01$, minimum reduced $\chi^2 = 4.28$). The rest wavelength for this object ranges from about 1305 Å to about 3764 Å.

Figure 5 shows fitting results for the quasar [HB89] 1331+170. As shown in the figure, the predicted flux is lower than the observed flux in the blue range indicating that this quasar is not reddened. From Table 2, one can also see that the best fit E_{B-V} values are negative for all three extinction curves, again indicating a slight mismatch between the template and the fitted quasar.

COMPARING DUST IN OTHER GALAXIES TO DUST IN OUR GALAXY

Table 2 shows the best flux normalization, best fit E(B-V), and the minimum reduced chi squared values for each extinction curve for each object. The highlighted minimum reduced chi squared values correspond to the best fit extinction curves for that quasar. The best fit E(B-V) values written in red correspond to a quasar that is reddened.

	NED Name	Extinction Curve	R_V Value	Best Flux Normalization	Best Fit E(B-V)	Minimum Reduced χ^2
1	PG 0003+158*	SMCbar	2.74	0.90	-0.08	4.8E-2
		LMC2	2.76	0.90	-0.05	5.3E-2
		MW	3.08	1.00	-0.01	5.5E-2
2	UM 321	SMCbar	2.74	25.0	-0.06	1.50
		LMC2	2.76	20.5	-0.10	1.56
		MW	3.08	20.0	-0.09	2.55
3	LBQS 0256-000	SMCbar	2.74	4.00	0.04	5.14
		LMC2	2.76	4.00	0.04	3.91
		MW	3.08	2.50	-0.06	3.87
4	3C 232***	SMCbar	2.74	95.5	0.10	68.5
		LMC2	2.76	140.0	0.18	68.4
		MW	3.08	139.0	0.13	79.9
5	MRK 0132	SMCbar	2.74	34.5	-0.02	6.21
		LMC2	2.76	31.0	-0.04	4.70
		MW	3.08	30.5	-0.04	4.61
6	[HB89] 1115+080C	SMCbar	2.74	30.0	-0.01	1.30
		LMC2	2.76	30.5	-0.01	1.75
		MW	3.08	32.5	-3.0E-8	1.97
7	PG 1206+459**	SMCbar	2.74	91.0	-3.0E-8	8.71
		LMC2	2.76	91.0	-3.0E-8	8.71
		MW	3.08	91.0	-3.0E-8	8.71
8	LBQS 1229-0207	SMCbar	2.74	25.0	0.06	2.78
		LMC2	2.76	32.5	0.12	2.68
		MW	3.08	44.5	0.17	2.45
9	PG 1241+176	SMCbar	2.74	65.0	0.02	5.61
		LMC2	2.76	65.0	0.02	5.75
		MW	3.08	65.5	0.02	5.94
10	SBS 1259+593***	SMCbar	2.74	89.0	-0.20	18.8
		LMC2	2.76	80.0	-0.15	45.0
		MW	3.08	80.0	-0.11	66.4
11	[HB89] 1331+170	SMCbar	2.74	38.0	-2.9E-8	4.47
		LMC2	2.76	35.9	-0.01	3.85
		MW	3.08	35.9	-0.01	4.26
12	PG 1338+416	SMCbar	2.74	35.0	0.01	1.68
		LMC2	2.76	36.5	0.02	1.62
		MW	3.08	35.0	0.01	1.61
13	UM 632	SMCbar	2.74	2.50	0.03	3.82
		LMC2	2.76	2.50	0.03	3.66

COMPARING DUST IN OTHER GALAXIES TO DUST IN OUR GALAXY

		MW	3.08	2.50	0.03	3.92
14	SDSSJ170100.61+641209.0***	SMCbar	2.74	21.5	-0.01	32.6
		LMC2	2.76	20.0	-0.02	32.7
		MW	3.08	20.0	-0.02	35.4
15	SBS 1704+608***	SMCbar	2.74	191.5	-0.05	39.2
		LMC2	2.76	180.0	-0.06	43.7
		MW	3.08	180.0	-0.05	49.8
16	OI363	SMCbar	2.74	35.0	-0.13	4.60
		LMC2	2.76	20.0	-0.25	4.89
		MW	3.08	20.0	-0.20	7.73

* For PG 0003+158, the minimum reduced χ^2 value is 0.048, which means it is a really good fit.

However, this object was not observed in SDSS, and the data available in the literature had no uncertainties. Therefore, the uncertainties were estimated, and these estimates could be underestimates of the true uncertainties, which may explain the low χ^2 value.

** For PG 1206+459, the minimum reduced χ^2 values are essentially identical for the Milky Way, LMC2, and SMCbar extinction curves. In any case, this matters little since this object is essentially unreddened.

*** For these objects, the smallest reduced chi squared minimum is high, indicating a poor fit. Thus, it is possible that the template spectrum does not fit the observed spectrum well and a different template may be needed.

The table above, Table 2, shows the best flux normalization, best fit E_{B-V} , and minimum reduced χ^2 values for each extinction curve on each quasar. The best fit E_{B-V} values that are positive indicate reddening; these values are shown in red in Table 2. The minimum reduced χ^2 values that are highlighted in yellow indicated the smallest value and correspond to extinction curve that best fits the quasar spectrum.

5 Conclusions

In this project 16 objects were analyzed as shown in Tables 1 and 2, all of which were in the optical region. Of those 16 objects, the best fit extinction curve of 9 of them was formally SMCbar. This means that the dust with the absorption redshifts in Table 1 are most similar to SMCbar. From Figure 1, we see that SMCbar is flat, it does not have a 2175 Å bump, and is steeper in the UV region. Thus, the dust for those 9 objects did not produce a 2175 Å bump and has a steeper UV rise. However, looking at the E(B-V) values in Table 2 for those objects, the values are relatively small. The object PG 1241+176 was the only object that had SMCbar as the best fit extinction curve as well as a positive E(B-V) value, which was also small. Milky Way and LMC2 were the best fit extinction curves for the rest of the objects in the table. The E(B-V) values were also either negative or relatively small for these objects. Therefore, we can conclude that there was no significant extinction or reddening and so there was not much dust in the foreground of those quasars. The negative E(B-V) values in these cases suggest a slight mismatch between the template spectrum and the fitted quasar spectrum.

From Table 2, there were 5 objects that had positive E(B-V) values, in which 3 of these objects have Mg II measurements as shown in Table 1. The other two objects have H I measurements including PG 1338+416 that has a small Mg II measurement. From these 5 objects, two had LMC2 as their formal best fit curve, two had Milky Way, and one had SMCbar. The objects with a positive E(B-V) value correspond to objects with various absorption redshifts. Two of the objects from Table 2 had an E(B-V) value that was greater than 0.15, which means that there was an adequate amount of reddening. Therefore, there is no significant correlation between the E(B-V) values and the absorption redshift for the dust in the foreground of each object. There are two objects in Table 2, SBS 1259+593 and OI363, that have very low E(B-V) values. For these

COMPARING DUST IN OTHER GALAXIES TO DUST IN OUR GALAXY

objects we do not sample regions shorter than 4000 Å in the rest wavelength, and thus we cannot see the effects of reddening.

Future work would include working on the spectra in the UV region as well on the infrared region. This means that the template for the infrared objects would be that from Hatzimagalou et al. (2005). For those objects that have infrared spectra, we will combine those with the optical spectra to obtain improved dust extinction estimates, and then examine any trends between the improved E(B-V) values and metallicity, H I column density or redshift.

References

- Cecchi-Pestellini, C., Mulas, G., Casu, S., Lati, M. A., Saija, R., Cacciola, A., Borghese, F., & Denti, P. (2011). Modeling Galactic Extinction. *Atti Della Accademia Peloritana Di Pericolanti*, 89(1). <https://doi.org/10.1478/CIV89SIP002>
- Cousin, M., Buat, V., Lagache, G., & Bethermin, M. (2019). G.A.S. *Astronomy & Astrophysics*, 627, A132. <https://doi.org/10.1051/0004-6361/201834674>
- Czerny, B., Li, J., Loska, Z., & Szczerba, R. (2004). Extinction due to amorphous carbon grains in red quasars from the Sloan Digital Sky Survey. *Monthly Notices of the Royal Astronomical Society*, 348(3), L54–L57. <https://doi.org/10.1111/j.1365-2966.2004.07590.x>
- Draine, B. T. (2003). Interstellar Dust Grains. *Annual Review of Astronomy and Astrophysics*, 41(1), 241–289. <https://doi.org/10.1146/annurev.astro.41.011802.094840>
- Draine, B. T., & Li, A. (2007). Infrared Emission from Interstellar Dust. IV. The Silicate-Graphite-PAH Model in the Post-Spitzer Era. *The Astrophysical Journal*, 657(2), 810–837. <https://doi.org/10.1086/511055>

COMPARING DUST IN OTHER GALAXIES TO DUST IN OUR GALAXY

- Hatziminaoglou, E., Pérez-Fournon, I., Polletta, M., Afonso-Luis, A., Hernán-Caballero, A., Montenegro-Montes, F. M., Lonsdale, C., Xu, C. K., Franceschini, A., Rowan-Robinson, M., Babbedge, T., Smith, H. E., Surace, J., Shupe, D., Fang, F., Farrah, D., Oliver, S., González-Solares, E. A., & Serjeant, S. (2005). Sloan Digital Sky Survey Quasars in the Spitzer Wide-Area Infrared Extragalactic Survey (SWIRE) ELAIS N1 Field: Properties and Spectral Energy Distributions. *The Astronomical Journal*, 129(3), 1198–1211. <https://doi.org/10.1086/428003>
- Jones, A. (2009). The role of dust in the interstellar medium: dust sources and dust evolution. *EAS Publications Series*, 34, 107–118. <https://doi.org/10.1051/eas:0934008>
- Masci, F. J., & Webster, R. L. (1999). Cosmological obscuration by galactic dust: effects of dust evolution. *Monthly Notices of the Royal Astronomical Society*, 305(4), 937–945. <https://doi.org/10.1046/j.1365-8711.1999.02471.x>
- Kulkarni, V. P., Torres-Garcia, L. M., Som, D., York, D. G., Welty, D. E., & Vladilo, G. (2011). Interstellar silicate dust in five quasar absorption systems. *The Astrophysical Journal*, 726(14), 15. <https://doi.org/10.1088/0004-637X/726/1/14>
- Juvela, M., Neha, S., Mannfors, E., Saajasto, M., Ysard, N., & Pelkonen, V.-M. (2020). Dust emission, extinction, and scattering in LDN 1642. *Astronomy & Astrophysics*, 643, A132. <https://doi.org/10.1051/0004-6361/202038611>
- Morgan, H. L., & Edmunds, M. G. (2003). Dust formation in early galaxies. *Monthly Notices of the Royal Astronomical Society*, 343(2), 427–442. <https://doi.org/10.1046/j.1365-8711.2003.06681.x>
- Mörtzell, E. (2013). Calibrating Milky Way dust extinction using cosmological sources. *Astronomy & Astrophysics*, 550, A80. <https://doi.org/10.1051/0004-6361/201220587>

COMPARING DUST IN OTHER GALAXIES TO DUST IN OUR GALAXY

Murphy, M. T., & Liske, J. (2004). Dust-reddening and gravitational lensing of SDSS QSOs due to foreground damped Lyman α systems. *Mon. Not. R. Astron. Soc.*, 354, L31–L36.

<https://doi.org/10.1111/j.1365-2966.2004.08374.x>

Srianand, R., Gupta, N., Petitjean, P., Noterdaeme, P., & Saikia, D. J. (2008). Detection of the 2175 Å extinction feature and 21-cm absorption in two MgII systems at $z \sim 1.3$. *Monthly Notices of the Royal Astronomical Society: Letters*, 391, L69–L73.

<https://doi.org/10.1111/j.1745-3933.2008.00558.x>

Sterken, V. J., Westphal, A. J., Altobelli, N., Malaspina, D., & Postberg, F. (2019). Interstellar Dust in the Solar System. *Space Science Reviews*, 215(7). <https://doi.org/10.1007/s11214-019-0607-9>

Tress, M., Ferreras, I., Pérez-González, P. G., Bressan, A., Barro, G., Domínguez-Sánchez, H., & Eliche-Moral, C. (2019). A deeper look at the dust attenuation law of star-forming galaxies at high redshift. *Monthly Notices of the Royal Astronomical Society*, 488(2), 2301–2311. <https://doi.org/10.1093/mnras/stz1851>

Triani, D. P., Sinha, M., Croton, D. J., Pacifici, C., & Dwek, E. (2020). The origin of dust in galaxies across cosmic time. *Monthly Notices of the Royal Astronomical Society*, 493(2), 2490–2505. <https://doi.org/10.1093/mnras/staa446>

Xue-cao, S., Xiang, P., Li-ming, D., Jian-guo, W., Peng, J., Chen-wei, Y., & Hong-yan, Z. (2020). Milky-Way-Like 2175 Å Dust Extinction Feature Observed toward the Quasar SDSS J0916+2921. *Chinese Astronomy and Astrophysics*, 44(2), 196–209.

<https://doi.org/10.1016/j.chinastron.2020.05.004>

COMPARING DUST IN OTHER GALAXIES TO DUST IN OUR GALAXY

Zhuravlev, V. V. (2020). Dynamic role of dust in formation of molecular clouds. *Monthly Notices of the Royal Astronomical Society*, 500(2), 2209–2226.

<https://doi.org/10.1093/mnras/staa3424>